

# AFM nanoindentation: tip shape and tip radius of curvature effect on the hardness measurement

L Calabri<sup>1</sup>, N Pugno<sup>2</sup>, C Menozzi<sup>1</sup> and S Valeri<sup>1,3</sup>

<sup>1</sup> CNR-INFM—National Research Center on nanoStructures and bioSystems at Surfaces (S3), Via Campi 213/a, 41100 Modena, Italy

<sup>2</sup> Department of Structural Engineering, Politecnico di Torino, Corso Duca degli Abruzzi 24, 10129 Torino, Italy

<sup>3</sup> Department of Physics, University of Modena and Reggio Emilia, via Campi 213/a, 41100 Modena, Italy

E-mail: [calabri.lorenzo@unimore.it](mailto:calabri.lorenzo@unimore.it)

Received 21 April 2008, in final form 4 July 2008

Published 6 November 2008

Online at [stacks.iop.org/JPhysCM/20/474208](http://stacks.iop.org/JPhysCM/20/474208)

## Abstract

AFM nanoindentation is nowadays not so widespread for the study of mechanical properties of materials at the nanoscale. ‘Nanoindenter’ machines are presently more accurate and more standardized. However, AFM could provide interesting features such as imaging the indentation impression right after the load application.

In this work a new method for nanoindentation via AFM is proposed. The use of AFM allows hardness measurement with standard sharp AFM probes and a simultaneous high-resolution imaging (which is not achievable with standard indenters—*cube corner* and *Berkovich*). How the shape of the indenter and the tip radius of curvature affect the hardness measurement is here analysed with three different approaches: experiments, numerical simulations and theoretical models. In particular the effect of the tip radius of curvature, which is not negligible for the real indenters, has been considered both in the nature of the indentation process, than in the practice of imaging with AFM.

A final theoretical model has been developed, that includes the effect of the tip radius of curvature as well as variable corner angle. Through this model we have been able to define a correction factor which permits us to evaluate the actual hardness of the material, once the radius of curvature of the tip is measured.

(Some figures in this article are in colour only in the electronic version)

## 1. Introduction

Over the last few years, interest in nanomechanics has increased considerably. In particular the characterization of the mechanical properties at the nanoscale has been studied intensively from a theoretical and experimental point of view, but the theoretical work strongly depends upon accurate experimental results. Nanoindentation techniques, in particular, have been extensively exploited by many researchers worldwide to study hardness, Young’s modulus and other mechanical properties of thin films and coatings [1–4]. The techniques have been widely investigated to understand their main features at the nanoscale.

The idea of nanoindentation arose from the necessity to measure the mechanical properties of very small volumes of materials. In principle, if a very sharp tip is used, the volume of material that is tested can be made arbitrarily small. However, in this case, it is very difficult to determine the indentation area. The hardness is in fact defined as the ratio between the maximum applied load ( $P_{\max}$ ) and the projected area of the indentation impression ( $A_p$ ). To evaluate this area, several depth sensing indentation (DSI) methods were developed [5–7], which allow an indirect measurement of  $A_p$  and permit one to evaluate hardness without imaging the indentation impression. In particular, most of the recent studies concerning material nanohardness are

based on the analysis of the load–displacement curves resulting from the nanoindentation test using the Oliver and Pharr (O–P) method [6–8].

The AFM approach to nanoindentation [4, 9], on the contrary, permits a direct measurement of the projected area of the indentation impression. As a matter of fact, although this technique is nowadays not so widespread, as ‘nanoindenter’ machines become ever more accurate and standardized, AFM could provide interesting features such as imaging the indentation impression right after the load application. With this approach it is possible to recognize the exact morphology of the indentation impression with high resolution at the nanoscale, measuring the actual value of the area  $A_p$ . This approach allows one to consider the presence of piled-up material, which is a major topic for indentation at the nanoscale [10, 11], that is usually neglected with the O–P approach and leads to an overestimation in the hardness value [12–14].

In the present paper a new method for nanoindentation is proposed. It allows hardness measurements with standard sharp AFM probes; the use of these probes enables simultaneous high-resolution imaging (which is not achievable with standard indenters—*cube corner* and *Berkovich*). It is in fact useful, in order to investigate the surface hardness at the nanoscale, to perform nanoindentation and subsequently image the corresponding surface modification using the AFM. How the shape of the indenter [15] and the tip radius of curvature affect the hardness measurement is analysed here to find a relationship between the measured hardness of a material, the corner angle of the pyramidal indenter and its tip radius of curvature. To experimentally understand this effect a photoresist material (*Microposit s1813 photo resists*) has been indented with focused ion beam (FIB) nanofabricated probes with different corner angles [15]. We then compared the results obtained experimentally with those obtained by numerical simulations and by theoretical models [16].

The comparison between these three approaches reveals a good agreement in the hardness behaviour even if an overestimation of the experimental results has been noticed at small corner angles [15]. This is related to the tip radius of curvature of real indenters, which is not negligible and affects the experimental results, both in the nature of the experimental procedure and in the process of imaging with AFM. The presence of a non-zero tip radius of curvature is ascribable to wear during the indent-imaging process or to manufacturing defects. It could affect the indentation process because the indenter, no longer ideal, will deform the specimen with a different geometry. However it could also affect the process of imaging, as the non-ideal tip will interact with the morphology, convoluting the asperities depending on its actual shape. For this reason the theoretical and numerical models were modified in order to consider these effects and to obtain a closer match between the experimental and numerical approaches. In this way we were also able to define a correction factor  $C$  which permits one to evaluate the actual hardness of the material, by filtering the experimental data.

## 2. Indentation shape effect

The indentation shape effect (IShE [15]) defines how the shape of the indenter affects the measurement of material hardness. It is obvious that, changing the shape of the indenter (and in particular the tip corner angle), the behaviour of the material penetration process changes.

In order to gain a basic knowledge of the IShE a full experimental analysis has been performed and reported in detail in a previous work [15]. In particular a series of nanoindentations were performed on a soft photoresist material (*Microposit s1813 photo resists*) using FIB nanofabricated silicon probes with different tip corner angle (figure 1). This set of indenters is formed by commercial silicon AFM tips (*MPP-11100-Tap300 Metrology Probes* from *Veeco*<sup>®</sup>) customized with an FIB facility. This kind of tip is made of silicon and consequently could not provide a high mechanical profile in terms of hardness and non-deformability. For this reason we decided to use them to indent a soft substrate such as a photoresist material, in order to keep a high ratio between the hardness of the indenter and the hardness of the sample. In this way the silicon tips, even if provided with a poor hardness value, will be basically non-deformable when pressed on the selected soft material. These three indenters are characterized by the equivalent corner angles reported in the caption of figure 1 for each probe.

The whole experimental investigation is performed using AFM nanoindentation. The instrument we used is a *Digital Instruments Enviroscope Atomic Force Microscope* by *Veeco*<sup>®</sup>. The experimentation consists of matrices of indentations performed for each probe under exactly the same conditions. The matrix is composed of twenty-five indentations and the applied load is of  $\sim 2000$  nN. This load is calculated from the photodetector voltage (1.6 V), multiplying this value by the cantilever spring constant and by the deflection sensitivity.

The hardness has been evaluated by a direct method, imaging the indentation impressions by the AFM technique right after the load application, using the same customized probes as used for the indentation phase. From the images, we were able to measure the projected area of the indentation impressions in a direct way and thus evaluate the hardness just by dividing the applied vertical load by this area.

The hardness values obtained with this method are reported in figure 2 (dots) where a higher statistic has been obtained in comparison with the results showed in [15], increasing the number of indentations on the same material. Then the effect of the indenter shape on the determination of hardness modulus was examined.

In parallel with the experimental investigation, the finite element method (FEM) has been used to simulate the indentation process. The numerical results in terms of hardness versus indenter corner angle are reported in figure 2 (black squares). Both the experimental and numerical results have been analysed using a general law for nanoindentation which has been recently proposed to the scientific community [16]. This law predicts how the material hardness depends on the geometry of the indenter and on the characteristics of the specimen material, correlating the macroscale hardness

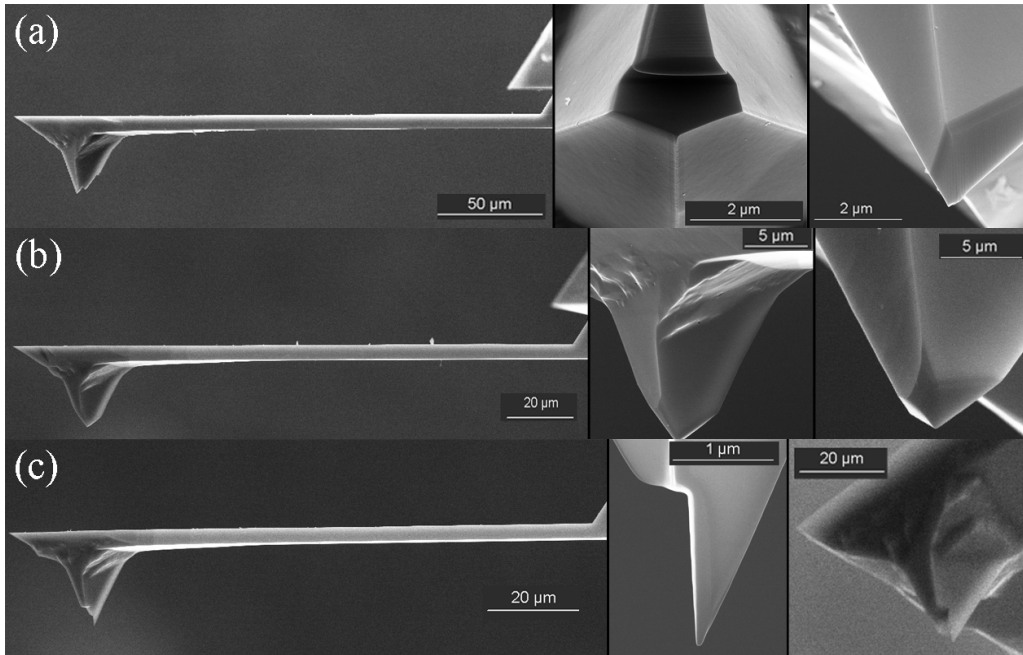


**Figure 1.** SEM images of the customized probes: (a) indenter no. 1—equivalent corner angle: 62°; (b) indenter no. 2—equivalent corner angle: 97°; (c) indenter no. 3—equivalent corner angle: 25°. (Reproduced from [18], with permission of IOP Publishing Ltd.)

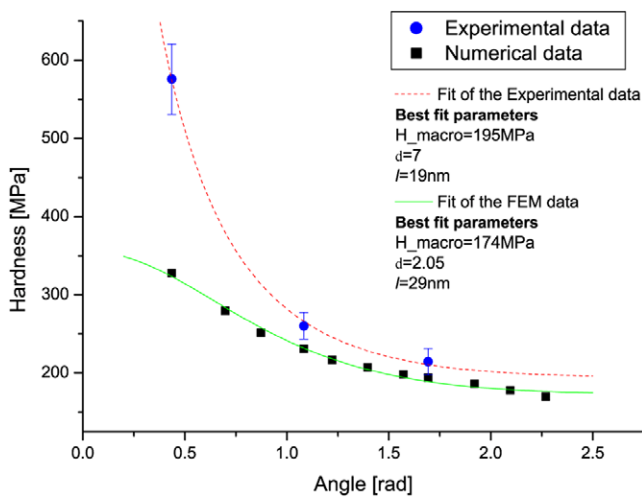


**Figure 2.** Comparison between the experimental results for the three customized indentation probes (dots) and numerical results (squares), theoretically interpolated (dashed and continuous line, respectively).

( $H_{macro}$ ), the nanoscale hardness ( $H_{nano}$ ) and the nominal hardness ( $H_{cone}$  for a conical indenter) of the specimen material, by means of the best-fit parameters  $\delta$  and  $l$ .  $\delta$  is just the ratio between  $H_{nano}$  and  $H_{macro}$ ; while  $l$  represents a characteristic material structural length, governing the transition from the nano to the macroscale.

The comparison between the experimental and numerical results (figure 2) reveals a good agreement in the hardness behaviour versus the indenter corner angle. Both the sets of data, in fact, show a precise theoretical fit, revealing the same trend (hardness decreases with increasing tip corner angle). This behaviour is in agreement with the theoretical approach,

which is based on dislocation motion theory. The dislocations movement, as reported by Pugno [16], is strongly affected by the shape of the indenter, resulting in a different hardness measurement.

Despite this trend similarity, the two approaches present a clear difference in the actual hardness values. In particular an overestimation of the experimental results is evident at small corner angles. This is connected to the fact that the tip radius of curvature of real indenters is not negligible and affects the experimental results, making the measured hardness values larger than the ideal ones. This effect is particularly evident for small corner angles.

In the present work we expanded the aforementioned investigation [15], focusing on the effect of the tip radius of curvature, which was found to be a major feature, affecting the experimental results in a remarkable way.

### 3. Tip radius of curvature: how to include this parameter

In the AFM indentation procedure, the radius of curvature at the tip affects the hardness measurement in two different ways: (i) it has an influence on the nature of the penetration process, as the indenter, no longer ideal, deforms the specimen with a different geometry; (ii) it affects the process of AFM imaging, as the non-ideal tip will interact with the morphology, convoluting the asperities depending on its actual shape. For this reason it is necessary to determine the real shape of the indenter (in terms of tip radius of curvature) and then to modify the theoretical and numerical models in order to consider this effect.

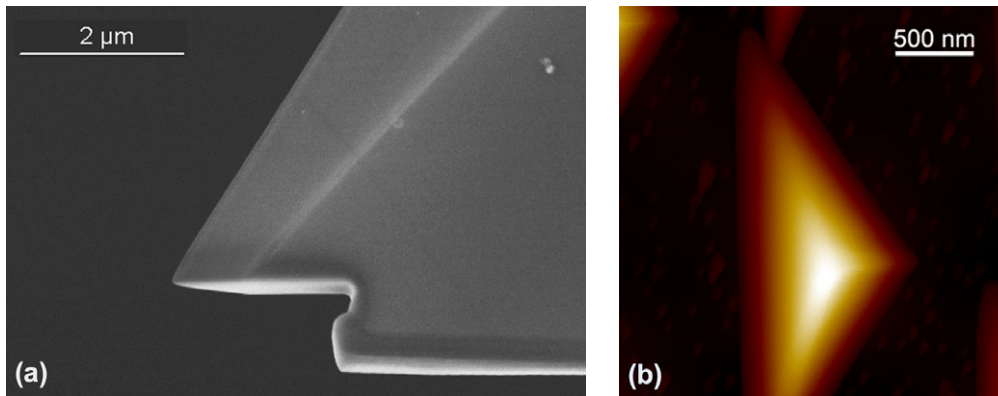


**Figure 3.** (a) SEM image of the customized probe no. 1; (b) AFM image on the calibration grid of the customized probe no. 1.

**Table 1.** Tip radius of curvature of the nanofabricated probes.

Indenter	Tip radius of curvature (nm)
Probe no. 1	21
Probe no. 2	26
Probe no. 3	25

### 3.1. Tip radius of curvature characterization

The topography of the customized indentation tips was obtained by a SEM microscope equipped with a SFEG electron source and also by an AFM working in tapping mode. Using the SEM we were able to directly obtain the geometry of the tip (figure 3(a)), even if the image obtained is a 2D projection of the tip. The result achieved in this way does not concern the actual three-dimensional structure of the system, but just a planar view of it.

Using the AFM it is possible to obtain a 3D topography of the tip (figure 3(b)), scanning the probe on a calibration grid (test grating *TGTI—NT-MDT*<sup>®</sup>), which is composed of an array of ultra-sharp tips. The image obtained in this way is three-dimensional and represents the actual shape of the indenter. Using the ‘tip characterization’ tool equipped with the SPIP<sup>TM</sup> software that we used for the AFM image analysis, we are able to precisely detect the tip radius of curvature of the three customized probes used for the nanoindentation procedure (table 1).

### 3.2. Numerical model

The FEM methodology is used here to simulate the indentation process. In particular we modified the numerical model, developed in a previous work [15], in order to consider in addition the effect of the tip radius of curvature in the hardness evaluation.

In this analysis we approach the numerical model as a nonlinear contact problem. Both the indenter and the specimen are considered bodies of revolution and the pyramid indenter is approximated by an axisymmetric cone (figure 4). In this way it is possible to avoid the high computing time associated with the three-dimensional nature of the problem, without introducing considerable errors.

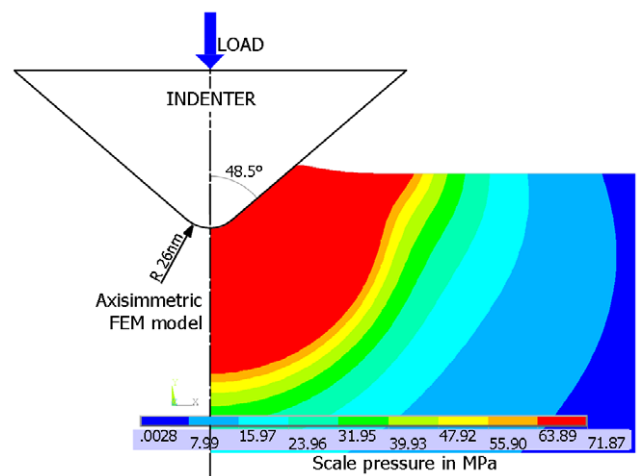


**Figure 4.** Stress distribution in the indentation model; the vertical arrow represents the applied load direction during the indentation process.

In the present model it is assumed that the indenter is perfectly rigid and the test material is isotropic, homogeneous, elasto-plastic with isotropic hardening behaviour, obeying the von Mises yield criterion; the material was assumed to be elastic–fully plastic, thus with no strain hardening. This is an acceptable assumption, since the material is a polymer-based photoresist which presents a perfectly plastic regime characterized by a constant yield stress [17].

The indentation process is simulated by moving the indenter with a downward–upward displacement (100 nm). This brings the indenter to push into the surface and then release, until it is free of contact with the specimen.

The indenter is modelled using the equivalent corner angles designed for the customized probes (62°, 97° and 25°) and using the tip radius of curvature obtained from the tip characterization (21, 26 and 25 nm—section 3.1).

### 3.3. Theoretical model

Assuming the presence of a non-vanishing tip radius of curvature ( $R$ ), the simplified tip geometry that we consider in order to find a theory which models this kind of problem is

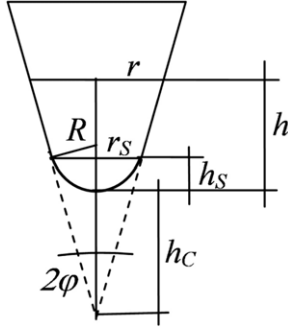


**Figure 5.** Conical indenter with worn spherical tip.

the one reported in figure 5. Note that geometrically  $h_s = R(1 - \sin \varphi)$ ,  $h_c = R(1 - \sin \varphi)/\sin \varphi$  and  $r$  depends on the depth of indentation  $h$  and it is:  $r = \sqrt{2Rh - h^2}$  for  $h \leq h_s$  or  $r = (h + h_c) \tan \varphi$  for  $h > h_s$ .

According to Pugno [16] the hardness related to the worn indenter will be given by:

$$H_{\text{cone}}(h, \varphi, R) = H_{\text{macro}} \sqrt{1 + \frac{\delta^2 - 1}{\delta^2 \ell^{-1} V/S(h, \varphi, R) + 1}}, \quad (1)$$

where:  $\delta = H_{\text{nano}}/H_{\text{macro}}$ ;  $\ell$ : characteristic material structural length, governing the transition from the nano to the macroscale;  $S$ : lateral (having height  $h$ ) minus the base (having radius  $r$ ) surface areas of the indentation;  $V$ : hemispherical volume with base surface identical to that of the indentation (radius  $r$ );  $H_{\text{cone}}$ : nominal hardness;  $H_{\text{macro}}$ : macrohardness;  $H_{\text{nano}}$ : nanohardness.

Thus the term  $\frac{S}{V}(h, \varphi, R)$  can be deduced by geometrical consideration as:

$$\frac{S}{V}(h, \varphi, R) = \begin{cases} \frac{3h^2}{2(2Rh - h^2)^{3/2}} & h \leq h_s \\ \frac{[(h + h_c)^2 - (h_s + h_c)^2](1/\sin \varphi - 1) \tan^2 \varphi + h_s^2}{2/3(h + h_c)^3 \tan^3 \varphi} & h > h_s. \end{cases} \quad (2)$$

Introducing (2) into (1) it is possible to obtain an expression for the material hardness as a function of: (i) depth of indentation, (ii) tip corner angle, and (iii) tip radius of curvature.

Note the continuity of the function  $S/V(h, \varphi, R)$  around  $h_s$  and note that  $S/V(h \gg R, \varphi, R) \equiv S/V(h, \varphi, R = 0)$ . This means that the role of the tip radius of curvature becomes negligible for large indentation depths. Obviously  $S/V(h \leq h_s, \varphi, R)$  is not a function of  $\varphi$ , just representing a pure spherical indentation.

Imagine performing experiments with an ideal tip (thus with  $R \rightarrow 0$ ), in order to measure the ideal material hardness  $H_{\text{ideal}} \equiv H(h, \varphi, R = 0)$ . Unfortunately we would experimentally measure  $H_{\text{measured}} = H(h, \varphi, R_{\text{exp}})$  and thus the ideal material hardness will be  $H_{\text{ideal}} = CH_{\text{measured}}$ , thus

**Table 2.** Tip radius of curvature correction factors for the nanofabricated probes.

Indenter	Correction factor $C$
Probe no. 1 ( $R = 21$ nm, $\varphi = 62^\circ$ )	1.156
Probe no. 2 ( $R = 24$ nm, $\varphi = 97^\circ$ )	1.840
Probe no. 3 ( $R = 26$ nm, $\varphi = 25^\circ$ )	1.036

the correction factor  $C$  will be defined as:

$$C = \frac{H(h, \varphi, R = 0)}{H(h, \varphi, R_{\text{exp}})}. \quad (3)$$

Since  $S/V(h, \varphi, R)$  (see (2)) increases with decreasing  $R$ , correction factors  $C$  larger than one are to be expected ( $C \geq 1$ ). For this reason, wear would imply hardness underestimation, in agreement with the finite element analyses (see figure 7(a)).

In particular introducing (1) and (2) into (3):

$$C(h, \varphi, R) = \sqrt{\frac{1 + \frac{\delta^2 - 1}{\delta^2 \ell^{-1} V/S(h, \varphi, 0 \text{ nm}) + 1}}{1 + \frac{\delta^2 - 1}{\delta^2 \ell^{-1} V/S(h, \varphi, R_{\text{exp}}) + 1}}} \quad (4)$$

which allows the deduction of the correction factors  $C$  for the nanofabricated probes used for the experimental part of this work (table 2).

### 3.4. Deconvolution of the indentation impressions

The presence of a radius of curvature at the tip in an AFM indentation probe affects not only the process of load application during the indentation, but also the process of AFM imaging, as the non-ideal tip will interact with the morphology, convoluting the asperities depending on its actual shape. For this reason, in order to overcome this problem, which could dramatically influence the AFM hardness results, we decided to geometrically deconvolute the AFM images, considering the tip radius of curvature that we measured during the topography characterization (section 3.1).

The software that we used to measure the indentation impression area (SPIP™ software), considers the ‘tangent height’ of the indentation (which is the depth of indentation) reduced by 10%, in order to avoid any roughness influence (see figure 6(a) where  $h$  is the 10% of the whole depth of indentation  $H$ ). In figure 6(a) the dashed line is the artefact image obtained by the AFM, while the black line is the ideal profile. Thus, considering the ‘tangent height’, the difference between the measured indentation impression and the ideal one is only related to  $x$  (figure 6(a), (b)), which could be obtained by geometrical considerations as  $x = R \cdot \cos \alpha$ , with  $\alpha = \arcsin(1 - \frac{h}{R})$ .

The actual projected area ( $A^1$ —hatched area in figure 6(b)) could be thus obtained from the measured one ( $A_p$ —pink area in figure 6(b)) with the following relation:

$$A^1 = \frac{\sqrt{3}}{4} \left( \sqrt{\frac{4A_p}{\sqrt{3}}} + 2\sqrt{3}x \right). \quad (5)$$

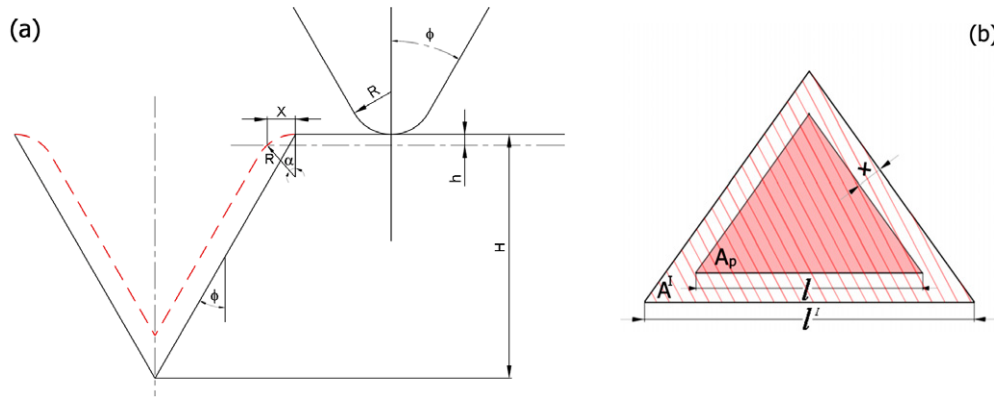


**Figure 6.** Schematic of the deconvolution process; (a) interaction during the AFM imaging phase between the tip and indentation impression; (b) projected area of the indentation impression.

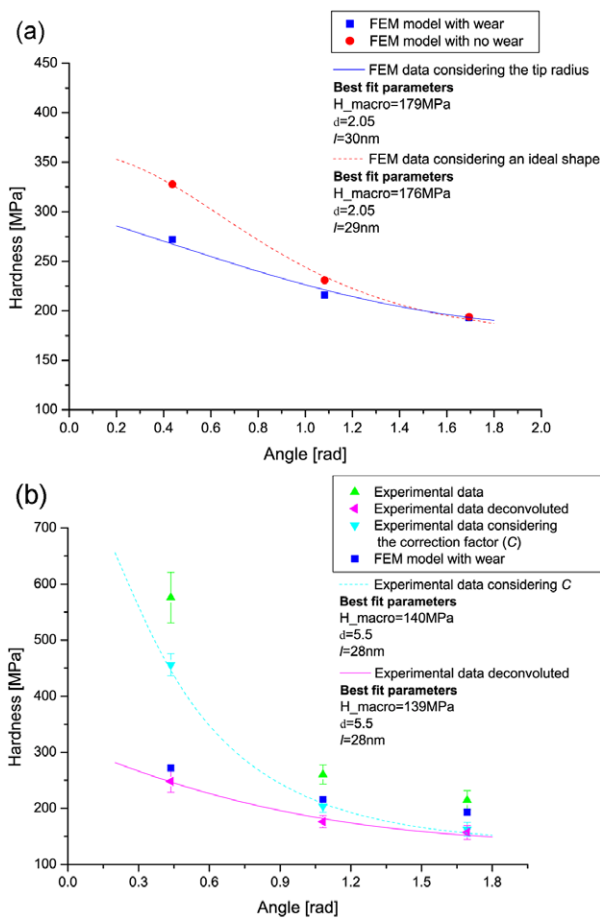


**Figure 7.** (a) Numerical hardness results considering in the FEM model an indenter with an ideal shape (dots) and with a worn shape (squares). The numerical data are theoretically interpolated (dashed and continuous line, respectively); (b) comparison between the experimental results deconvoluted (lateral triangles) and the numerical data (squares). In the same graph are also reported the raw experimental results (up triangles) and the experimental results considering the correction factor  $C$  (down triangles).

#### 4. Results

In figure 2 direct comparison between the experimental and numerical results is reported. This comparison reveals

a good agreement in the hardness behaviour although an overestimation of the experimental results is evident at small corner angles as a consequence of the tip radius of curvature effect. We should thus expect that the presence of a rounded tip on the indenter gives an overestimation of the measured hardness, justifying the gap between the experimental and numerical results. On the contrary, as highlighted from numerical simulations (figure 7(a)) and confirmed from theoretical models (section 3.3), the effect of the tip radius of curvature on the hardness measurement in terms of the penetration process is opposite. The hardness values, numerically evaluated modelling the indenter as ideal (figure 7(a)—dots), is in fact higher than that those evaluated using a worn tip (figure 7(a)—squares). These numerical data have also been fitted with the theoretical relation (1), considering in the first case (dashed curve) a vanishing tip radius ( $R = 0$ ) and in the second case (continuous curve) the actual tip radii of the three customized probes (table 1). The best-fit parameters reported in the inset of figure 7(a) have exactly the same values for the two interpolations, confirming that the theoretical approach perfectly agrees with the numerical one.

The mismatch observed in figure 2 is therefore not ascribable to the tip radius of curvature effect on the indentation process, but it is ascribable to this effect on the AFM imaging process. As reported in section 3.4, in fact, the measured projected area of an indentation impression is slightly smaller than the real one, because of the convolution effect of the AFM tip. Thus, considering this effect and correcting the measured areas with the procedure described in section 3.4, we are able to estimate the actual value of the material hardness. In figure 7(b) the raw experimental data (up triangles) versus the deconvoluted experimental data (lateral triangles) are reported. It is possible to observe a difference, especially for small corner angles, in the hardness values. In the same graph the numerical data of the modelled worn indenter are also reported (squares), showing a now excellent agreement in the trend of the hardness curve over the whole range of the corner angles chosen. The final macrohardness  $H_{macro}$  obtained as a best-fit parameter from the experimental data ( $\sim 140$  MPa) is slightly underestimated with respect to the

numerical value ( $\sim 180$  MPa) and to the value deduced from the literature ( $\sim 150$ – $200$  MPa). The actual value of the material hardness obtained experimentally is anyway very close to the value from literature and the underestimation can be related to a difference in the material properties used as input parameters in the numerical model (the material described in literature and used in the numerical model is presumably not exactly the same as the material used for the experiment).

Finally we have also filtered the deconvoluted experimental results (lateral triangles) by the correction factor  $C$ , theoretically evaluated for the three customized probes (table 2). These corrected data are also reported in figure 7(a) (down triangles). The results filtered by the deconvolution process (lateral triangles) and those corrected by the correction factor  $C$  (down triangles) have both been theoretically interpolated (continuous and dashed curve, respectively). The result of this process reveals a complete agreement in terms of best-fit parameters (inset of figure 7(b)), which are exactly the same, confirming that the theoretical model is self-consistent.

## 5. Conclusion

An AFM-based nanoindentation study on tip shape and tip radius of curvature effect on the hardness measurement is proposed here. Three different-shaped indentation probes have been designed and realized with a FIB machine. A complete experimental analysis has been performed with these indenters in order to quantify how the hardness measurement is affected by two important parameters: (i) the tip corner angle [15] and (ii) the tip radius of curvature of the nanoindenter. A FEM model has also been designed in order to understand the process of indentation better and it has been further developed in order to take into account the tip radius of curvature effect. In parallel a theoretical approach, based on a recent theory on nanoindentation [16], has been optimized for a worn indenter. These two approaches allow one to interpret the experimental results, showing that the differences between the experimental, the numerical and the theoretical data are related mainly to the tip radius of curvature effect, which affects not only the penetration process during indentation, but also, and in a significant way, the AFM imaging process. The hardness has been in fact obtained in a direct way, measuring the projected area of the indentation impression by the AFM high-resolution images. A geometrically deconvolution process has been utilized in order to correct the systematic error related to the tip radius of curvature effect.

The results obtained allowed us to deduce a theoretical relation which links the measured hardness value with the shape of the indenter and with its tip radius of curvature. In particular a correction factor  $C$  has been defined to take into account this last effect, allowing the correction of the experimental results in order to find the actual material hardness during an AFM indentation process.

## Acknowledgments

The authors would like to acknowledge the FIB laboratory (a CNR-INFM-S3 Lab).

This work has been supported by Regione Emilia Romagna (LR no. 7/2002, PRRITT misura 3.1A) and Net-Lab SUP&RMAN (Hi-Mech district for Advanced Mechanics Regione Emilia Romagna).

## References

- [1] Li X and Bhushan B 2002 A review of nanoindentation continuous stiffness measurement technique and its applications *Mater. Charact.* **48** 11–36
- [2] Saha R and Nix W D 2002 Effects of the substrate on the determination of thin film mechanical properties by nanoindentation *Acta Mater.* **50** 23–38
- [3] Zhang F, Saha R, Huang Y, Nix W D, Hwang K C, Qu S and Li M 2007 Indentation of a hard film on a soft substrate: strain gradient hardening effects *Int. J. Plast.* **23** 25–43
- [4] Bhushan B and Koinkar V N 1994 Nanoindentation hardness measurements using atomic force microscopy *Appl. Phys. Lett.* **64** 1653–55
- [5] Doerner M F and Nix W D 1986 A method for interpreting the data from depth-sensing indentation instruments *J. Mater. Res.* **1** 601–09
- [6] Oliver W C and Pharr G M 1992 An improved technique for determining hardness and elastic modulus using load and displacement sensing indentation experiments *J. Mater. Res.* **7** 1564
- [7] Oliver W C and Pharr G M 2004 Measurement of hardness and elastic modulus by instrumented indentation: advances in understanding and refinements to methodology *J. Mater. Res.* **19** 1
- [8] Pharr G M, Oliver W C and Brotzen F R 1992 On the generality of the relationship among contact stiffness, contact area, and elastic modulus during indentation *J. Mater. Res.* **7** 613
- [9] Withers J R and Aston D E 2006 Nanomechanical measurements with AFM in the elastic limit *Adv. Colloid Interface Sci.* **120** 57–67
- [10] Miyake K, Fujisawa S, Korenaga A, Ishida T and Sasaki S 2004 The effect of pile-up and contact area on hardness test by nanoindentation *Japan. J. Appl. Phys.* **43** 4602–5
- [11] Beegan D, Chowdhury S and Laugier M T 2005 Work of indentation methods for determining copper film hardness *Surf. Coat. Technol.* **192** 57–63
- [12] Poole W J, Ashby M F and Fleck N A 1996 Micro-hardness of annealed and work-hardened copper polycrystals *Scr. Mater.* **34** 559–64
- [13] Pharr G M 1998 *Mater. Sci. Eng. A* **253** 151–9
- [14] Saha R, Xue Z, Huang Y and Nix W D 2001 Indentation of a soft metal film on a hard substrate: strain gradient hardening effects *J. Mech. Phys. Solids* **49** 1997–2014
- [15] Calabri L, Pugno N, Rota A, Marchetto D and Valeri S 2007 Nanoindentation shape-effect: experiments, simulations and modeling *J. Phys.: Condens. Matter* **19** 395002–13
- [16] Pugno N M 2007 A general shape/size-effect law for nanoindentation *Acta Mater.* **55** 1947–53
- [17] Yoshimoto K, Stoykovich M P, Cao H B, de Pablo J J, Nealey P F and Drugan W J 2004 A two-dimensional model of the deformation of photoresist structures using elastoplastic polymer properties *J. Appl. Phys.* **96** 1857–65
- [18] Calabri L, Pugno N, Rota A, Marchetto D and Valeri S 2007 *J. Phys.: Condens. Matter* **19** 395002